ACS OMEGA

Article

Cite This: ACS Omega 2020, 5, 1902−1910

Design of Rubber Composites with Autonomous Self-Healing Capability

Saul Utrera-Barrios, Marianella Hernández Santana,* Raquel Verdejo, and Miguel A. López-Manchado

Institute of Polymer Science and Technology (ICTP-CSIC), Juan de la Cierva 3, 28006 Madrid, Spain

Supporting Information

ABSTRACT: The development of self-healing rubbers is currently under investigation as a strategy to promote their reuse and, hence, reduce their waste. However, autonomous, multicycle self-healing rubbers with good mechanical properties have so far proven difficult to achieve. Here, mechanically robust composites based on epoxidized natural rubber (ENR) and thermally reduced graphene oxide (TRGO) were successfully designed and prepared with a high healing efficiency of up to 85% at room temperature without applying external stimuli. The incorporation of TRGO not only improves the mechanical performance in more than 100% in relation to pristine ENR but also promotes the hydrogen bonding interactions with the rubber. This leads to a homogenous dispersion of TRGO within the ENR matrix, which further increases its self-healing capability.

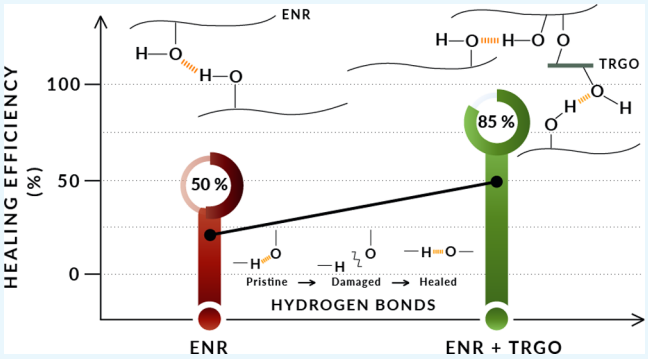

1. INTRODUCTION

In recent years, the inefficient disposal and handling of polymer waste is considered to be one of the most serious problems for the environment, and in particular, elastomers are at a disadvantage compared to thermoplastics because they cannot be easily reprocessed. Therefore, the scientific community has made significant efforts to mitigate rubber waste through the development of new ways of devulcanization[1,2] or through their use as fillers in other systems.[3,4] However, rubber waste is still a pressing issue to be solved. An alternative and actual strategy to overcome this limitation is by conferring self-healing capability to elastomers, thus promoting their reuse.

Self-healing is defined as the ability of a material to recover or repair damage.[5] It can be classified as extrinsic and intrinsic. In extrinsic self-healing materials, a healing agent is dispersed in the matrix and is released when some type of damage occurs.[6−8] These materials present the drawback of being limited to a single cycle of self-healing.[9] In the case of intrinsic self-healing materials, recovery after damage is achieved through supramolecular interactions, such as polar interactions and hydrogen bonds,[10−14] disulfide bonds,[15−17] other bonds from reversible chemistry (like Diels−Alder[18] and transesterification reactions[19−21]), metal−ligand and ionic interactions,[22] shape memory,[23] and combinations between them.[24,25] The disadvantages of these materials are, to date, twofold: they need an external stimulus, such as pressure or temperature, to activate these interactions[9] and their mechanical properties are not optimal. Nonetheless, these methodologies have resulted in the development of systems with high self-healing efficiencies.

A strategy to improve the mechanical properties of self-healing elastomers is the inclusion of fillers. Cao et al.[12] used tunicate cellulose nanocrystals (t-CNs) in epoxidized natural rubber (ENR) compounds, achieving efficiencies of up to 85% but requiring 20 parts per hundred parts of rubber (phr) of the filler. Hernández Santana et al.[17] developed a styrene−butadiene rubber compound incorporating ground tire waste, achieving a self-healing efficiency of up to 50%, due to the exchange of disulfide bonds. Furthermore, they improved the mechanical properties of the compounds by 80% with the incorporation of a coupling agent without adversely affecting the self-healing efficiency. Li et al.[26] prepared a complex polymeric system with self-healing capability, based on a polymer synthesized in situ with furan and maleimide groups and graphene oxide functionalized with furfurylamine and maleic acid. Such a system promoted crosslinking by the Diels−Alder chemistry, enabling healing efficiencies of up to 90%. The procedure, however, required a 110 °C temperature and complex chemistry. Huang et al.[23] designed a thermoplastic elastomer based on ENR, polylactic acid, and ferrous ferric oxide with a healing efficiency up to 70%, assisted by the shape memory effect. The use of thermally reduced graphene oxide (TRGO) has been pursued in different rubber matrices,[26−30] particularly NR[31] with different self-healing

Received: October 21, 2019
Accepted: December 9, 2019
Published: January 17, 2020

DOI: 10.1021/acsomega.9b03516
ACS Omega 2020, 5, 1902−1910

protocols, including infrared light, electricity, and electromagnetic wave. These studies proved that the addition of TRGO improved the healing efficiencies to over 98% with just 5 wt % of TRGO.[30] In NR, TRGO reinforced the matrix and achieved healing efficiencies for a tensile strength of up to 62% with just 1.00 phr.[31] However, to the best knowledge of the authors, no publications were found related to the self-healing capability of the ENR−TRGO system.

Currently, the research of elastomers with intrinsic self-healing capability faces a great challenge: to achieve simultaneously (a) autonomous self-healing, i.e., without any external stimuli and (b) a positive balance between healing and mechanical performance, which have been reported as antagonistic properties.[32] Therefore, the purpose of this study was the development of ENR reinforced with in-house synthesized TRGO with autonomous self-healing capability. In the first stage, various compounds of ENR were prepared with different contents of epoxy units and dicumyl peroxide (DCP) to optimize the healing capability. This optimized system was later used as a matrix in ENR−TRGO nanocomposites. The reason to select TRGO was related to the presence on its surface of remaining hydroxyl, carbonyl, and epoxy groups from its synthesis.[33] These functional groups were aimed at both improving the filler−matrix interactions and contributing to the self-healing through the formation of hydrogen bonds.

2. RESULTS AND DISCUSSION

2.1. Optimization of ENR Compounds with Self-Healing Capability. The six ENR compounds for the first stage were designed with different contents of epoxy units and three concentrations of DCP, as shown in Table 1.

Table 1. ENR Compounds Expressed in phr

ingredient	F1	F2	F3	F4	F5	F6
ENR 25	100	100	100			
ENR 50				100	100	100
DCP	0.8	1.2	1.6	0.8	1.2	1.6

In the second stage, ENR−TRGO nanocomposites were designed with three different contents of TRGO: 0.25 phr for FX-A; 0.50 phr for FX-B, and 1.00 phr for FX-C, where "*X*" denotes the number of the optimized compound in the first stage.

ENR can present different levels of epoxide groups randomly dispersed along the isoprene backbone of the natural rubber. We selected two levels of epoxidation, 25 and 50 mol %, ENR 25 and ENR 50, respectively, and analyzed its self-healing capability. Supporting Information 1 shows the curing curves for the six ENR compounds. In both elastomeric matrices, an increase in the maximum torque values (M_H) is observed with the increase of the DCP content, well related to the increase in crosslink density of the materials.

The curing parameters can be correlated with the mechanical properties by means of tensile tests, which are one of the most used characterization techniques in elastomers. The stress−strain curves and parameters of the ENR compounds are shown in Supporting Information 2. Accordingly, the values of modulus at low deformations (M_{100} and M_{300}) increased with the peroxide content because of the increase in crosslink density.[34] Higher tensile strength was also observed in ENR 25 systems as the DCP content increased. This result is consistent with the trend in the maximum torque values and the crosslink density. On the other hand, the presence of a higher content of *cis*-1,4 polyisoprene units of the NR (which crystallizes by deformation) provides a remarkable reinforcing capacity.[35] For the compounds with ENR 50, the tensile strength (σ_R) increased with the peroxide content and the elongation at break (ε_R) tended to decrease. This behavior is also associated with the higher crosslink density, which stiffens the material and decreases its ability to deform.[34]

Figure 1 shows the results of the tensile test after the self-healing protocol at 70 °C, as well as the efficiency of that protocol as a measure of the retention of mechanical properties. The obtained results can be linked to two variables: first, the content of epoxy units and second, the peroxide content. A higher healing efficiency was observed for ENR 50, with values of (53 ± 4)% in tensile strength and (56 ± 2)% in elongation at break, which is attributed to the higher concentration of epoxy units. On the other hand, the results show a decrease in the self-healing efficiency with the increase of the peroxide content, which is related to the increase in the crosslink density. It is important to note that healing occurs if the polymer chains have certain degree of mobility to diffuse. This mobility then enables the restoration of the bonds and, hence, is impeded with high crosslink density.[32]

No results were found to compare directly these results to those of others using ENR as a matrix, due to many variables involved in the self-healing process (epoxidation content,

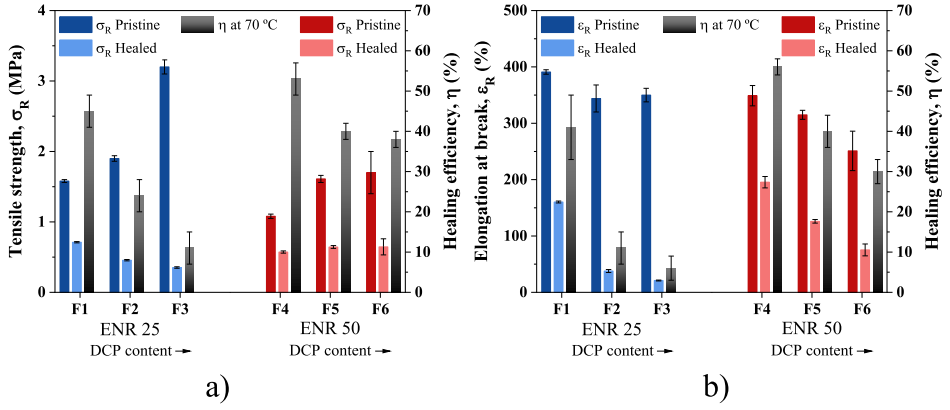

Figure 1. Healing efficiency of ENR compounds after applying a healing treatment at 70 °C based on: (a) tensile strength; (b) elongation at break.

DOI: 10.1021/acsomega.9b03516
ACS Omega 2020, 5, 1902−1910

crosslink density, time and cure temperature, curing system, and others). However, two studies report the healing efficiency for unfilled ENR under different conditions. According to Cao et al.,[12] the percentage retention of tensile strength in ENR 40 (with 40% of epoxidation content) was 48% but with a lower amount of DCP, 0.5 phr. Additionally, Nie et al.[14] report a slightly lower efficiency of 42% for tensile strength and just 12% for elongation at break. Nevertheless, their composites were not vulcanized with any conventional crosslink agent. These results reflect the importance of vulcanization in the properties of rubber composites and the self-healing process.

There are two common reactions during the vulcanization of a diene rubber with organic peroxides: (1) the abstraction of hydrogen adjacent to the double bond to form the C−C bond, which generates the crosslinked structure and (2) the rupture of the double bond and a chain growth (a kind of polymerization). The ENR case involves a third competing reaction: the ring-opening of epoxy groups that form hydroxyl groups (−OH).[36] These groups have been suggested to create an effective thermoreversible crosslinked supramolecular network in the ENR matrix.[12,37] Thus, the higher concentration of epoxy units results in a higher concentration of hydroxyl groups, which in turn increases the formation of hydrogen bonds and thereby the self-healing capability. Scheme 1 presents the described chemical route followed during the ring-opening reaction of the epoxy group (at 160 °C) and the self-healing mechanism by the formation of hydrogen bonds. Recently, this healing mechanism has also been suggested in NR, where Sattar et al.[38] combined the effect of hydrogen bonds, within the NR proteins and lipids, with metal−ion interactions and achieved healing efficiencies of 52% for the tensile strength at 50 °C in an unfilled compound.

Scheme 1. Proposed Scheme of Self-Healing Mechanism in ENR Compounds

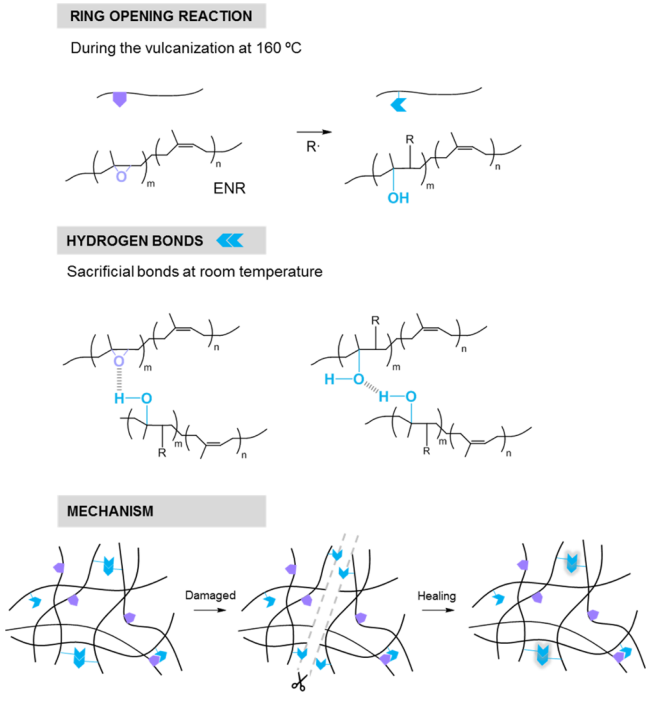

The existence of these functionalities and hydrogen bonds can be observed by infrared spectroscopy in the attenuated total reflectance (ATR) mode. Figure 2 shows the spectra of F1 and F4 (the spectra of all six ENR compounds are presented in the Supporting Information 3). The peaks associated with the *cis*-1,4 polyisoprene unit are identified at 2960, 2920, and 2860 cm^{-1} for the stretching vibration (str. vib.) of −CH, at 1660 cm^{-1} for the bending (bend. vib.) of C═C, and at 1450, 1370, and 825 cm^{-1} for the bending of CH_2, CH_3, and ═CH, respectively. Regarding the epoxy group, its characteristic peak is identified at 870 cm^{-1} that corresponds to the ring stretching vibration and suggests that not all rings have been opened during vulcanization. A small peak at 1730 cm^{-1} is also observed and is associated with minor carboxylic groups derived from the epoxidation reaction of the NR.[12] The bands of the hydroxyl groups are observed in the range between 3200 and 3500 cm^{-1}.[39] The different epoxy content is clearly observed in the band at 870 cm^{-1} as increases its intensity in F4. Furthermore, the bands associated with the *cis*-1,4 polyisoprene unit at 1660 and 825 cm^{-1} decrease and become broader and more diffuse. Moreover, differences are also observed in the hydroxyl bands, which intensify at 3480 cm^{-1} in ENR 50. This is associated with the presence of intermolecular interactions, such as hydrogen bonds and free hydroxyl groups. Another important change in the spectra occurs in the bands that appear in the interval between 1110 and 900 cm^{-1}, associated with the products derived from the opening of the epoxy ring (other than hydroxyl), mainly of the C−O−C (str. vib.) type.[36,39]

To optimize the healing conditions, the temperature was reduced from 70 °C to room temperature. The results obtained are summarized in Figure 3. No significant variation on the self-healing capability was observed. For ENR 25, no changes in the healing efficiency were detected; while for ENR 50, the values at 70 °C were slightly higher with a variation of less than 10%. Hence, F4 (ENR 50) healed at 25 °C was selected as the optimal compound and healing protocol.

2.2. Development of ENR−TRGO Nanocomposites with Self-Healing Capability. The effect of the TRGO in the curing process was analyzed as a function of the TRGO content. The Supporting Information 1 shows the curing curves of ENR−TRGO nanocomposites. An increase of M_H was observed in the nanocomposites with TRGO compared to the base compound (F4), which is ascribed to the reinforcing capacity of the filler.[40] Additionally, M_H increases with the loading content of TRGO up to 0.50 phr and subsequently stabilizes. This trend could be attributed to possible agglomerations at 1 phr of TRGO, which would hinder the reinforcing capacity of the TRGO. Other studies have reported this fact at similar concentrations.[41−44]

In filled elastomers, the crosslink density determined by the equilibrium swelling method is considered as an indirect measurement of the filler−rubber interactions. There is an increase in the crosslink density, consistent with the M_H value, except in F4-C that decreases, which could be a consequence of the agglomerate formation. Scanning electron microscopy (SEM) images also suggest the presence of such agglomerates in this sample (Figure 4), where large lamellar structures are observed at high magnifications.

The study of the interactions in the ENR−TRGO nanocomposites was completed with the determination of the viscoelastic properties, via dynamic mechanical analysis (DMA), and the so-called Payne Effect. According to Payne,[45,46] there are four contributions to the reinforcement of a filled elastomer: the first derived from its crosslink density;

DOI: 10.1021/acsomega.9b03516
ACS Omega 2020, 5, 1902−1910

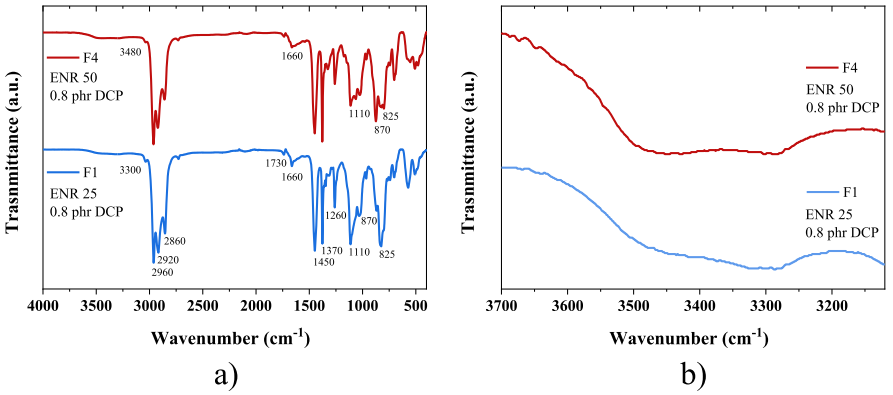

Figure 2. ATR spectra of F1 and F4 compounds: (a) general spectrum, (b) magnification in the hydroxyl groups band.

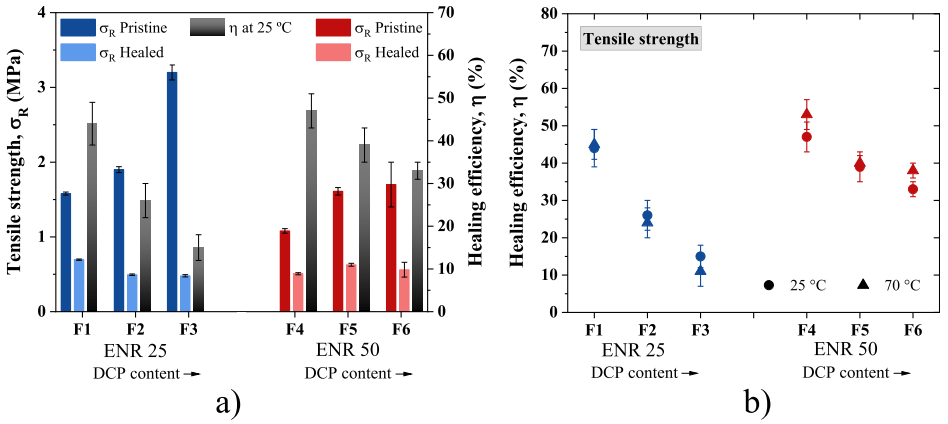

Figure 3. (a) Healing efficiency of ENR compounds at 25 °C; (b) healing efficiency at different temperatures.

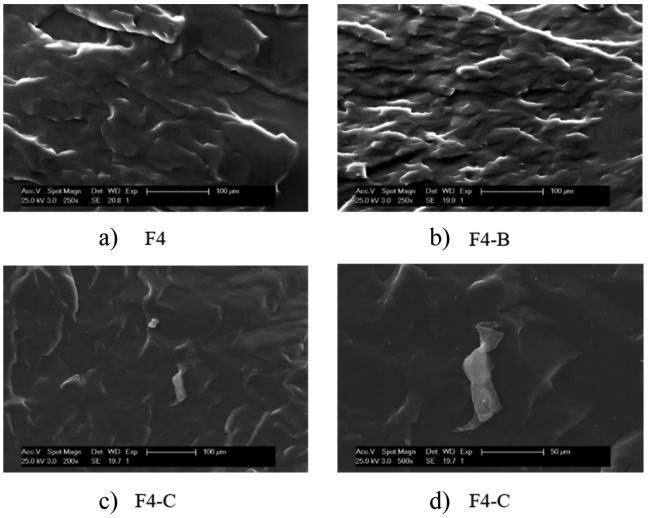

Figure 4. SEM photomicrographs of the ENR−TRGO nanocomposites: (a) F4—250×, (b) F4-B—250×, (c) F4-C—250×, and (d) F4-C—500×.

the second, the hydrodynamic effect of the filler; the third, the rubber−filler interactions; and, finally, the filler−filler interactions. The first three are independent of the deformation, whereas the last one is not. This dependence is quantified through the reduction of the storage modulus (E') when applying a deformation. When the weak interactions between the fillers are broken, portions of the elastomer trapped between these filler particles are released, increasing mobility and resulting in a decrease of E'. The quantification of this effect is then used to confirm the formation of agglomerates (filler−filler interactions) in a nanocomposite.[47−49] Figure 5

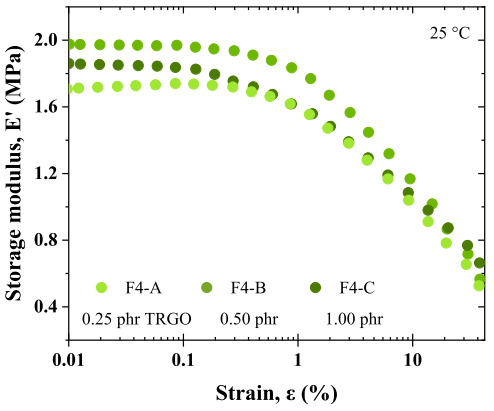

Figure 5. Study of the Payne effect by DMA.

shows the results by DMA. The increase in the E' plateau at low deformations is associated with an increase in stiffness through the incorporation of TRGO; however, compound F4-C deviates from this trend, which is associated with lower interactions with the matrix and greater filler−filler interactions (agglomerates), which is also corroborated by the earlier start of the E' drop.

Finally, the characterization of the mechanical properties of the nanocomposites was carried out. The Supporting

DOI: 10.1021/acsomega.9b03516
ACS Omega 2020, 5, 1902−1910

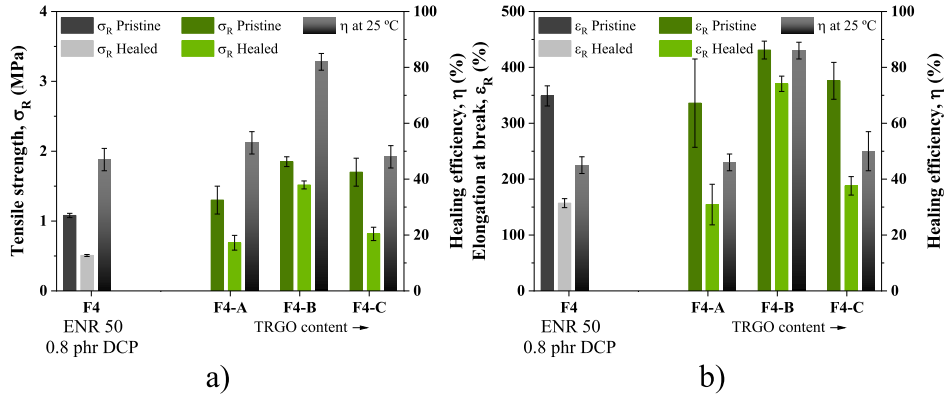

Figure 6. Healing efficiency of ENR−TRGO nanocomposites based on: (a) tensile strength; (b) elongation at break.

Scheme 2. Proposed Scheme of Self-Healing Mechanism in ENR−TRGO Nanocomposites

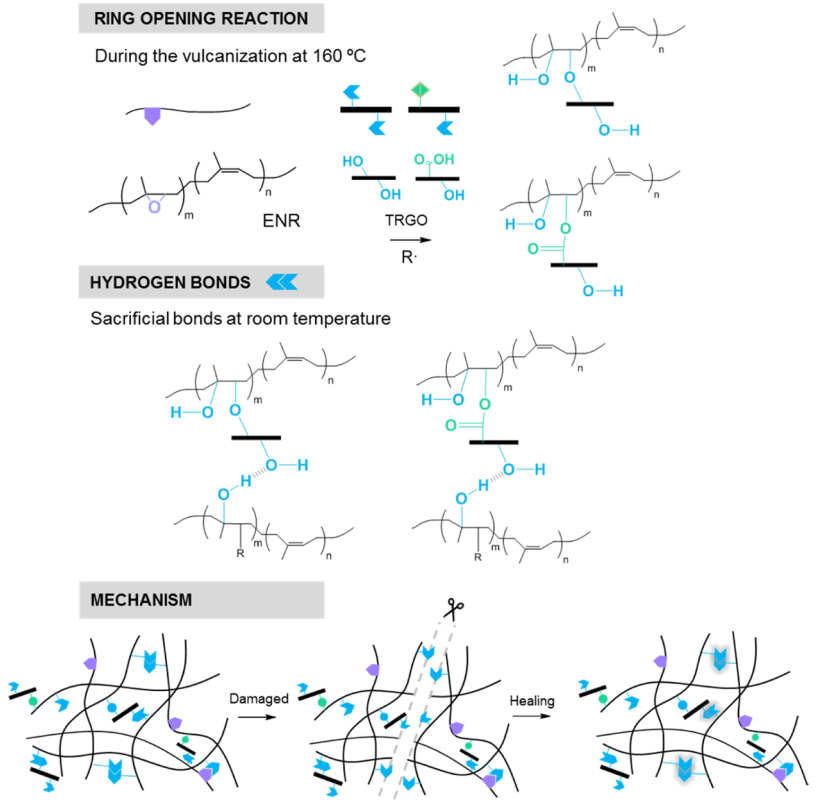

Information 4 summarizes the parameters derived from the stress−strain curves of the ENR−TRGO compounds. The stress at low deformations (M_{100} and M_{300}) increases as a function of the TRGO content due to the rise of hardness generated by the presence of a rigid solid in the soft matrix. Tensile strength also increases linearly with the nanofiller content, as a result of the good interaction between TRGO and the ENR matrix, reaching a maximum in the compound with better dispersion, F4-B.

Figure 6 shows the results of the tensile test of the ENR−TRGO nanocomposites after applying the self-healing protocol at 25 °C, as well as the healing efficiency as a measure of the recovery of the mechanical properties. For comparative purposes, the results of F4 previously presented are also included. TRGO increases the healing capability as a function of loading fraction, except for F4-C. Such a decrease in healing efficiency is ascribed to the formation of agglomerates. F4-B exhibits the greatest healing efficiency, with (82 ± 3)% in tensile strength and (86 ± 3)% in elongation at break. Supporting Information 5 shows the stress−strain curves of F4-B before and after healing protocol. Chen and co-workers have reported similar healing efficiencies using ENR 40 and different bio-based fillers.[12,14,21,37] Their results showed efficiencies of, on average, 85% for the tensile strength but required high loading fractions, 20 wt %, to achieve it and to obtain decent mechanical properties. In our investigation, we have achieved comparable mechanical reinforcement and self-healing efficiency to those systems reported in the literature but with an important decrease in the filler content. This substantial improvement could be a consequence of the good compatibility of TRGO with ENR and the higher formation of hydrogen bonds at room temperature. Scheme 2 shows the proposed reactions that could be occurring during the vulcanization and the self-healing mechanism.

DOI: 10.1021/acsomega.9b03516
ACS Omega 2020, 5, 1902−1910

As mentioned above, the epoxy ring opens during the vulcanization and forms two radicals. The radical associated with the oxygen atom usually becomes a hydroxyl group, while the carbon radical of the main chain pairs with some derivative of the decomposition units of the vulcanization agent or with the radical of another chain, as shown in Scheme 1. The incorporation of TRGO results in the formation of hydrogen bonds between its functional groups and the radicals derived from the rupture of the epoxy ring. To verify this fact, the ATR study of the nanocomposites was carried out, as shown in Figure 7. In the zone of the triplet, at 1100 cm^{-1}, the variations

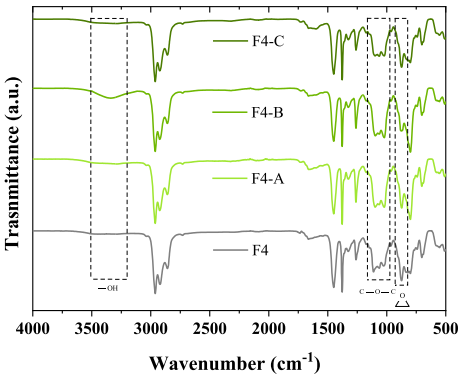

Figure 7. ATR spectra of the ENR−TRGO nanocomposites.

derived from the rupture of the epoxy ring are observed, being this change evident for F4-B. This could be associated with the formation of C−O−C structures that contribute to the reinforcement.[39] This fact is corroborated with the decrease of the intensity of the peak at 870 cm^{-1} and with the increase of the hydroxyl group band that also shifts to 3350 cm^{-1}. This displacement can be associated with the formation of intermolecular hydrogen bonds that can be sacrificial at room temperature and contribute directly to the self-healing capability. The shift to higher wavenumbers of the hydroxyl bands was observed by She et al.[40] and was also ascribed to the formation of hydrogen bonds between the ENR and oxygenated groups in the TRGO sheets. On the other hand, changes in the range between 840 and 800 cm^{-1} would be associated with the addition of TRGO.[39]

The self-healing capability was also followed at the microscopic level by optical profilometry. A scratch was made on the surface of the samples, and the same self-healing protocol was applied. Figure 8 shows the scratch profiles of F3 (sample with the lower self-healing efficiency at macroscopic level), F4 (base compound), and F4-B (sample with the higher self-healing efficiency at macroscopic level), before and after the healing protocol. The area between profiles is understood as the portion recovered, which will have a viscoelastic contribution (associated with the ENR) and another to the self-healing. In this way, the healing efficiency can be estimated from the relationship between the areas.[9] According to Vega et al.,[50] this technique provides one of the most suitable parameters to quantify the self-healing efficiency with a low experimental error. The results show comparable values to those achieved by the recovery of tensile properties (4% for F3, 68% for F4 and 88% for F4-B), confirming the healing capability. Furthermore, our results confirm the observation of Tanasi et al.[18] who proposed that the healing process starts from the bottom up.

3. CONCLUSIONS

ENR−TRGO composites with a high healing efficiency of up to 85% at room temperature were successfully prepared. Healing is achieved through the existence of hydrogen bonds and a supramolecular network. In addition, the incorporation of only 0.5 phr of TRGO improves the mechanical properties in more than 100% in relation to pristine ENR.

In summary, we demonstrate a conceptual framework to improve, simultaneously, the overall mechanical performance and healing ability of rubber nanocomposites, without applying an external stimulus and at room temperature. These results open the path to the development of other elastomeric materials in which the inclusion of nanofillers in small amounts

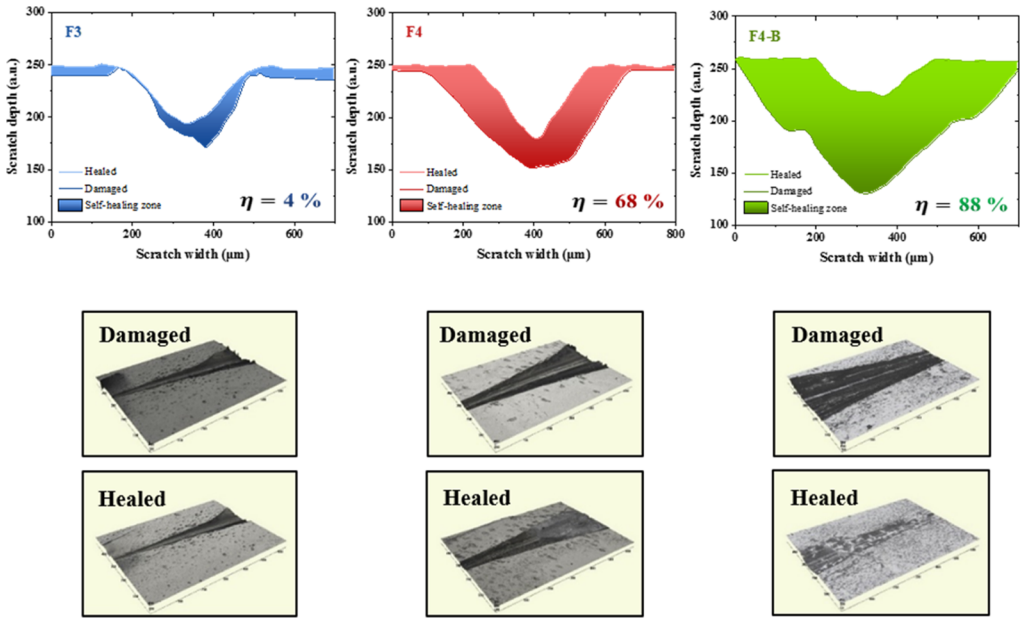

Figure 8. Optical scratch profiles before and after applying the self-healing protocol.

DOI: 10.1021/acsomega.9b03516
ACS Omega 2020, 5, 1902−1910

appears as a good alternative to overcome the trade-off between mechanical/structural performance and healing ability.

4. EXPERIMENTAL SECTION

4.1. Materials. Two grades of ENR were used with 25 and 50% of epoxy units (EKOPRENA 25 and EKOPRENA 50, respectively). Figure 9 shows the chemical structure of ENR,

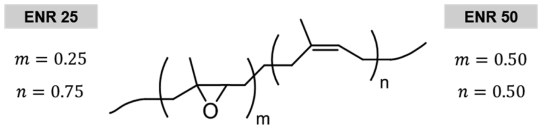

Figure 9. Chemical structure of ENR.

and Table 2 summarizes their technical specifications. The vulcanization system, bis(1-phenyl-1-methylethyl)peroxide ($C_{18}H_{22}O_2$), also known as DCP, was obtained from Merck KGaA.

Table 2. Technical Specifications of the Commercial Grades EKOPRENA 25 and EKOPRENA 50

specifications	units	EKOPRENA 25 (ENR 25)	EKOPRENA 50 (ENR 50)
epoxidation content	mol %	25 ± 2	50 ± 2
Mooney viscosity[a]	MU	70 − 100	70 − 100
glass transition temperature	°C	−45 ± 2	−20 ± 2

[a]ML (1 + 4) 100 °C.

Graphite powder (G), with a particle size of less than 20 μm, from Merck KGaA, was used to synthesize TRGO. Fuming nitric acid (HNO_3), 100% extra pure, and 99% potassium chlorate ($KClO_3$), reactive grade, were purchased from Merck KGaA and Acros Organics, respectively.

4.2. Synthesis and Characterization of TRGO. The synthesis of graphite oxide was carried out using the Brödie's method, followed by the exfoliation and thermal reduction under inert atmospheres at 1000 °C. Briefly, the fuming nitric acid was cooled to 0 °C in a cryostat bath, and then the graphite powder was added. Next, the potassium chlorate was slowly added, and the reaction mixture was stirred for 21 h at 0 °C. Finally, the mixture was diluted in distilled water and brought to neutral pH. After the thermal exfoliation and reduction, the obtained TRGO was stored in an airtight container. A detailed account of the reaction procedure can be found elsewhere.[33,51] Supporting Information 6 presents the characterization of the synthesized TRGO.

4.3. Preparation of ENR Compounds. The mixing was carried out in a two-roll mixer Comerio Ercole S. P. A., of 15 cm in diameter, 30 cm in length and friction ratio between rolls of 1:1.5 for 20 min. The equipment was maintained with a constant cooling system to avoid excessive heating during mixing and to prevent scorch. The rubber was passed through the rollers for mastication for 10 min. Then, DCP was added and transversal cuts were made to the band to promote the homogenization and good distribution of the additives. The final bands were stored in a refrigerator, at least 72 h before use. Mixing of the nanocomposites was also done in the two-roll mixer. The same procedure described was followed, incorporating the TRGO 8 min after initiating the mixing.

The vulcanization of the compounds was carried out in a hydraulic press Gumix, at 160 °C and a pressure of 200 bar. Five degasses were made to avoid the formation of bubbles, and subsequently, the test pieces were cut with the necessary dimensions for the different experimental techniques.

4.4. Characterization of the ENR Compounds.

4.4.1. Rheometric Properties. An oscillating disc rheometer from Alpha Technologies, model RPA 2000, was used for the rheological characterization of the prepared compounds. The samples were placed between polyester films on an oscillating disc with 1° amplitude at 160 °C for 120 min. The equipment recorded the torque generated by applying a shear deformation as a function of time, yielding the curing curves of the compounds, from which the curing time was obtained at 90% of the maximum torque (t_{90}).

4.4.2. Crosslink Density. Swelling measurements were performed on five squared samples, of 20 mm side and 2 mm thickness, for each compound. Once their mass in air was measured, they were introduced in a toluene bath, with enough separation and avoiding friction with the bottom of the container to minimize physical barriers that hinder diffusion. After 72 h, samples were weighted after extraction and after evaporation of the solvent until it reached a constant value at room temperature. The crosslink density (ν) was estimated by the Flory−Rehner relationship,[52,53] according to eq 1

$$\nu = -\frac{\ln(1 - V_R) + V_R + \mu V_R^{\,2}}{V_o\left(V_R^{\,1/3} - \frac{V_R}{2}\right)} \quad (1)$$

where V_o is the molar volume of toluene (106.20 cm^3/mol), μ is the Flory−Huggins interaction parameter between the rubber and toluene (0.42), and V_R is the volume fraction of rubber, estimated according to eq 2

$$V_R = \frac{\frac{m_1}{D} - V_F}{\frac{m_1}{D} - V_F + \left(\frac{m_2 - m_3}{D_S}\right)} \quad (2)$$

where m_1 is mass in air, m_2 is mass after extraction of the solvent, m_3 is mass after evaporation of the solvent, D is the density of the formulation, D_S is the density of the toluene (0.87 g/cm^3), and V_F is the volume fraction of the TRGO.

4.4.3. Scanning Electron Microscopy. The TRGO dispersion in the ENR matrix was observed by means of an environmental SEM, Phillips, model XL30 with a tungsten filament with an acceleration voltage of 25 kV, after sputter-coating with gold. The analysis was made on the surface derived from the cryogenic fracture of a sample of each compound of interest.

4.4.4. Fourier Transform Infrared Spectroscopy. The changes in the functional groups produced during the vulcanization of the nanocomposites were studied by infrared spectroscopy in the ATR mode using a PerkinElmer spectrometer, model UATR Two from 400 to 4000 cm^{-1}, with a resolution of 4 cm^{-1}.

4.4.5. Mechanical Properties. The determination of the mechanical properties was carried out in an Instron universal testing machine, model 3366, at room temperature. At least five dog-bone shape samples (type III) were tested according to UNE-ISO 37:2013 standard, using a cross-head speed of 200 mm/min and a distance between clamps of 35 mm. The tensile stress, also referred to as modulus, at 100, 300, and

DOI: 10.1021/acsomega.9b03516
ACS Omega 2020, 5, 1902−1910

500% deformation (M_{100}, M_{300}, M_{500}), tensile strength (σ_R) and elongation at break (ε_R) were recorded.

4.4.6. Self-Healing Protocol. The two broken sections of tested tensile tests were manually put in contact, and a minimum pressure was applied for 5 min to ensure adequate contact. The healing process was carried out for 24 h under two conditions: a group of samples at 70 °C and another group at room temperature. Once healed, they were re-tested according to the tensile test procedure previously described. The healing efficiency (η) was calculated as a measure of the recovery of tensile properties, according to eq 3

$$\eta(\%) = 100\frac{P_{healed}}{P_{pristine}} \quad (3)$$

where $P_{pristine}$ and P_{healed} is the property before and after the healing protocol.

4.4.7. Optical Profilometry. A surface scratch was made with a razor blade to the samples. The evolution of the scratch closure was followed with a Zeta-20 optical profilometer from Zeta Instruments. Photomicrographs were taken with a magnification of 20× and the depth profile of the crack was analyzed, taking care of its calculation in the same position in the damaged state and in the healed state.

4.4.8. Viscoelastic Properties. The study of the Payne effect was carried out in a dynamic rheometer DMA Q800 of TA Instruments. The tension configuration was used to perform strain sweeps between 0.01 and 40% at a frequency of 1 Hz and a temperature of 25 °C.

■ ASSOCIATED CONTENT

Supporting Information

The Supporting Information is available free of charge at https://pubs.acs.org/doi/10.1021/acsomega.9b03516.

Curing curves and crosslink density of ENR compounds and ENR−TRGO nanocomposites; mechanical properties of ENR compounds; infrared spectra of ENR compounds; mechanical properties of ENR−TRGO nanocomposites; stress−strain curves of F4-B before and after healing protocol; and characterization of TRGO (PDF)

■ AUTHOR INFORMATION

Corresponding Author

*E-mail: marherna@ictp.csic.es.

ORCID

Saul Utrera-Barrios: 0000-0003-4604-2305

Marianella Hernández Santana: 0000-0002-0609-3485

Author Contributions

S.U.-B: Conceptualization, Methodology, Experimental, Validation, Data curation, Formal analysis, Writing—original draft, Writing—review & editing. M.H.S.: Conceptualization, Methodology, Resources, Validation, Data curation, Writing—review & editing, Supervision. R.V.: Conceptualization, Validation, Writing—review & editing. M.A.L.-M.: Conceptualization, Validation, Writing—review & editing.

Funding

This work was funded in part by a research contract (MAT2015-73392-JIN) and Ramon y Cajal contract (RYC-2017-22837) of the Ministry of Science, Innovation and Universities of Spain.

Notes

The authors declare no competing financial interest.

■ ACKNOWLEDGMENTS

The authors acknowledge the Ministry of Science, Innovation and Universities of Spain for a research contract (MAT2015-73392-JIN) and M. Hernández Santana for a Ramón y Cajal contract (RYC-2017-22837).

■ REFERENCES

(1) Ghorai, S.; Bhunia, S.; Roy, M.; De, D. Mechanochemical devulcanization of natural rubber vulcanizate by dual function disulfide chemicals. *Polym. Degrad. Stab.* **2016**, *129*, 34−46.

(2) Aoudia, K.; Azem, S.; Aït Hocine, N.; Gratton, M.; Pettarin, V.; Seghar, S. Recycling of waste tire rubber: Microwave devulcanization and incorporation in a thermoset resin. *Waste Manag.* **2017**, *60*, 471−481.

(3) Ramarad, S.; Khalid, M.; Ratnam, C. T.; Chuah, A. L.; Rashmi, W. Waste tire rubber in polymer blends: A review on the evolution, properties and future. *Prog. Mater. Sci.* **2015**, *72*, 100−140.

(4) Sienkiewicz, M.; Janik, H.; Borzędowska-Labuda, K.; Kucińska-Lipka, J. Environmentally friendly polymer-rubber composites obtained from waste tyres: A review. *J. Clean. Prod.* **2017**, *147*, 560−571.

(5) Ghosh, S. K. *Self-Healing Materials: Fundamentals, Design Strategies, and Applications*, 1st ed.; Wiley-VCH: Weinheim, 2009; pp 1−68.

(6) White, S. R.; Sottos, N. R.; Geubelle, P. H.; Moore, J. S.; Kessler, M. R.; Sriram, S. R.; Brown, E. N.; Viswanathan, S. Autonomic healing of polymer composites. *Nature* **2001**, *409*, 794.

(7) Blaiszik, B. J.; Sottos, N. R.; White, S. R. Nanocapsules for self-healing materials. *Compos. Sci. Technol.* **2008**, *68*, 978−986.

(8) Bekas, D. G.; Baltzis, D.; Paipetis, A. S. Nano-reinforced polymeric healing agents for vascular self-repairing composites. *Mater. Des.* **2017**, *116*, 538−544.

(9) Hager, M. D.; Greil, P.; Leyens, C.; van der Zwaag, S.; Schubert, U. S. Self-Healing Materials. *Adv. Mater.* **2010**, *22*, 5424−5430.

(10) Zhang, H.; Xia, H.; Zhao, Y. Poly(vinyl alcohol) Hydrogel Can Autonomously Self-Heal. *ACS Macro Lett.* **2012**, *1*, 1233−1236.

(11) Rahman, M. A.; Sartore, L.; Bignotti, F.; Di Landro, L. Autonomic Self-Healing in Epoxidized Natural Rubber. *ACS Appl. Mater. Interfaces* **2013**, *5*, 1494−1502.

(12) Cao, L.; Yuan, D.; Xu, C.; Chen, Y. Biobased, self-healable, high strength rubber with tunicate cellulose nanocrystals. *Nanoscale* **2017**, *9*, 15696−15706.

(13) Guadagno, L.; Vertuccio, L.; Naddeo, C.; Calabrese, E.; Barra, G.; Raimondo, M.; Sorrentino, A.; Binder, W. H.; Michael, P.; Rana, S. Self-healing epoxy nanocomposites via reversible hydrogen bonding. *Composites, Part B* **2019**, *157*, 1−13.

(14) Nie, J.; Mou, W.; Ding, J.; Chen, Y. Bio-based epoxidized natural rubber/chitin nanocrystals composites: Self-healing and enhanced mechanical properties. *Composites, Part B* **2019**, *172*, 152−160.

(15) Hernández, M.; Grande, A. M.; Dierkes, W.; Bijleveld, J.; Van Der Zwaag, S.; García, S. J. Turning vulcanized natural rubber into a self-healing polymer: Effect of the disulfide/polysulfide ratio. *ACS Sustainable Chem. Eng.* **2016**, *4*, 5776−5784.

(16) Yang, Y.; Lu, X.; Wang, W. A tough polyurethane elastomer with self-healing ability. *Mater. Des.* **2017**, *127*, 30−36.

(17) Hernández Santana, M.; Huete, M.; Lameda, P.; Araujo, J.; Verdejo, R.; López-Manchado, M. A. Design of a new generation of sustainable SBR compounds with good trade-off between mechanical properties and self-healing ability. *Eur. Polym. J.* **2018**, *106*, 273−283.

(18) Tanasi, P.; Hernández Santana, M.; Carretero-González, J.; Verdejo, R.; López-Manchado, M. A. Thermo-reversible crosslinked natural rubber: A Diels-Alder route for reuse and self-healing properties in elastomers. *Polymer* **2019**, *175*, 15−24.

DOI: 10.1021/acsomega.9b03516
ACS Omega 2020, 5, 1902−1910

(19) Qiu, M.; Wu, S.; Tang, Z.; Guo, B. Exchangeable interfacial crosslinks towards mechanically robust elastomer/carbon nanotubes vitrimers. *Compos. Sci. Technol.* **2018**, *165*, 24−30.
(20) Xu, C.; Cui, R.; Fu, L.; Lin, B. Recyclable and heat-healable epoxidized natural rubber/bentonite composites. *Compos. Sci. Technol.* **2018**, *167*, 421−430.
(21) Cao, L.; Fan, J.; Huang, J.; Chen, Y. A robust and stretchable cross-linked rubber network with recyclable and self-healable capabilities based on dynamic covalent bonds. *J. Mater. Chem. A* **2019**, *7*, 4922−4933.
(22) Zhang, Z. F.; Liu, X. T.; Yang, K.; Zhao, S. G. Design of Coordination-Crosslinked Nitrile Rubber with Self-Healing and Reprocessing Ability. *Macromol. Res.* **2019**, *27*, 803−810.
(23) Huang, J.; Cao, L.; Yuan, D.; Chen, Y. Design of Novel Self-Healing Thermoplastic Vulcanizates Utilizing Thermal/Magnetic/Light-Triggered Shape Memory Effects. *ACS Appl. Mater. Interfaces* **2018**, *10*, 40996−41002.
(24) Liu, J.; Liu, J.; Wang, S.; Huang, J.; Wu, S.; Tang, Z.; Guo, B.; Zhang, L. An advanced elastomer with an unprecedented combination of excellent mechanical properties and high self-healing capability. *J. Mater. Chem. A* **2017**, *5*, 25660−25671.
(25) Lee, S.-H.; Shin, S.-R.; Lee, D.-S. Self-healing of cross-linked PU via dual-dynamic covalent bonds of a Schiff base from cystine and vanillin. *Mater. Des.* **2019**, *172*, 107774.
(26) Li, G.; Xiao, P.; Hou, S.; Huang, Y. Rapid and efficient polymer/graphene based multichannel self-healing material via Diels-Alder reaction. *Carbon* **2019**, *147*, 398−407.
(27) Wang, C.; Liu, N.; Allen, R.; Tok, J. B.-H.; Wu, Y.; Zhang, F.; Chen, Y.; Bao, Z. A Rapid and Efficient Self-Healing Thermo-Reversible Elastomer Crosslinked with Graphene Oxide. *Adv. Mater.* **2013**, *25*, 5785−5790.
(28) Zhan, Y.; Meng, Y.; Li, Y. Electric heating behavior of flexible graphene/natural rubber conductor with self-healing conductive network. *Mater. Lett.* **2017**, *192*, 115−118.
(29) Li, Y.; Gao, F.; Xue, Z.; Luan, Y.; Yan, X.; Guo, Z.; Wang, Z. Synergistic effect of different graphene-CNT heterostructures on mechanical and self-healing properties of thermoplastic polyurethane composites. *Mater. Des.* **2018**, *137*, 438−445.
(30) Huang, L.; Yi, N.; Wu, Y.; Zhang, Y.; Zhang, Q.; Huang, Y.; Ma, Y.; Chen, Y. Multichannel and Repeatable Self-Healing of Mechanical Enhanced Graphene-Thermoplastic Polyurethane Composites. *Adv. Mater.* **2013**, *25*, 2224−2228.
(31) Hernández, M.; Bernal, M. M.; Grande, A. M.; Zhong, N.; van der Zwaag, S.; García, S. J. Effect of graphene content on the restoration of mechanical, electrical and thermal functionalities of a self-healing natural rubber. *Smart Mater. Struct.* **2017**, *26*, 085010.
(32) Hernández Santana, M. H.; den Brabander, M.; García, S.; van der Zwaag, S. Routes to Make Natural Rubber Heal: A Review. *Polym. Rev.* **2018**, *58*, 585−609.
(33) Botas, C.; Álvarez, P.; Blanco, P.; Granda, M.; Blanco, C.; Santamaría, R.; Romasanta, L. J.; Verdejo, R.; López-Manchado, M. A.; Menéndez, R. Graphene materials with different structures prepared from the same graphite by the Hummers and Brodie methods. *Carbon* **2013**, *65*, 156−164.
(34) Coran, A. Y. Vulcanization. *Science and Technology of Rubber*; Elsevier, 2005; pp 321−366.
(35) Ikeda, Y.; Kato, A.; Kohjiya, S.; Nakajima, Y. *Rubber Science*; Springer: Singapore, 2018; pp 1−220.
(36) Krainoi, A.; Kummerlöwe, C.; Nakaramontri, Y.; Vennemann, N.; Pichaiyut, S.; Wisunthorn, S.; Nakason, C. Influence of critical carbon nanotube loading on mechanical and electrical properties of epoxidized natural rubber nanocomposites. *Polym. Test.* **2018**, *66*, 122−136.
(37) Xu, C.; Nie, J.; Wu, W.; Zheng, Z.; Chen, Y. Self-healable, recyclable and strengthened epoxidized natural rubber/carboxymethyl chitosan bio-based composites with hydrogen bonding supramolecular hybrid network. *ACS Sustainable Chem. Eng.* **2019**, *7*, 15778.
(38) Sattar, M. A.; Gangadharan, S.; Patnaik, A. Design of Dual Hybrid Network Natural Rubber-SiO2 Elastomers with Tailored Mechanical and Self-Healing Properties. *ACS Omega* **2019**, *4*, 10939−10949.
(39) Socrates, G. *Infrared and Raman Characteristic Group Frequencies*, 3rd ed.; John Wiley & Sons, LTD: England, 2001; pp 1−347.
(40) She, X.; He, C.; Peng, Z.; Kong, L. Molecular-level dispersion of graphene into epoxidized natural rubber: Morphology, interfacial interaction and mechanical reinforcement. *Polymer* **2014**, *55*, 6803−6810.
(41) Yaragalla, S.; Kalarikkal, N.; Thomas, S. Chemistry associated with natural rubber-graphene nanocomposites and its effect on physical and structural properties. *Ind. Crops Prod.* **2015**, *74*, 792−802.
(42) Yaragalla, S.; Chandran, C. S.; Kalarikkal, N.; Subban, R. H. Y.; Chan, C. H.; Thomas, S. Effect of reinforcement on the barrier and dielectric properties of epoxidized natural rubber-graphene nanocomposites. *Polym. Eng. Sci.* **2015**, *55*, 2439−2447.
(43) Aguilar-Bolados, H.; Lopez-Manchado, M. A.; Brasero, J.; Avilés, F.; Yazdani-Pedram, M. Effect of the morphology of thermally reduced graphite oxide on the mechanical and electrical properties of natural rubber nanocomposites. *Composites, Part B* **2016**, *87*, 350−356.
(44) Mohamed, A.; Ardyani, T.; Abu Bakar, S.; Sagisaka, M.; Umetsu, Y.; Hamon, J. J.; Rahim, B. A.; Esa, S. R.; Abdul Khalil, H. P. S.; Mamat, M. H.; King, S.; Eastoe, J. Rational design of aromatic surfactants for graphene/natural rubber latex nanocomposites with enhanced electrical conductivity. *J. Colloid Interface Sci.* **2018**, *516*, 34−47.
(45) Payne, A. R. The dynamic properties of carbon black-loaded natural rubber vulcanizates. Part I. *J. Appl. Polym. Sci.* **1962**, *6*, 57−63.
(46) Payne, A. R. The dynamic properties of carbon black loaded natural rubber vulcanizates. Part II. *J. Appl. Polym. Sci.* **1962**, *6*, 368−372.
(47) Wang, M.-J. The role of filler networking in dynamic properties of filled rubber. *Rubber Chem. Technol.* **1999**, *72*, 430−448.
(48) Fröhlich, J.; Niedermeier, W.; Luginsland, H.-D. The effect of filler-filler and filler-elastomer interaction on rubber reinforcement. *Composites, Part A* **2005**, *36*, 449−460.
(49) Yang, R.; Song, Y.; Zheng, Q. Payne effect of silica-filled styrene-butadiene rubber. *Polymer* **2017**, *116*, 304−313.
(50) Vega, J. M.; Grande, A. M.; Van der Zwaag, S.; Garcia, S. J. On the role of free carboxylic groups and cluster conformation on the surface scratch healing behaviour of ionomers. *Eur. Polym. J.* **2014**, *57*, 121−126.
(51) Brodie, B. C. XIII. On the atomic weight of graphite. *Philos. Trans. R. Soc. London* **1859**, *149*, 249−259.
(52) Flory, P. J.; Rehner, J., Jr Statistical Mechanics of Cross-Linked Polymer Networks I. Rubberlike Elasticity. *J. Chem. Phys.* **1943**, *11*, 512−520.
(53) Flory, P. J. Statistical Mechanics of Swelling of Network Structures. *J. Chem. Phys.* **1950**, *18*, 108−111.

DOI: 10.1021/acsomega.9b03516
ACS Omega 2020, 5, 1902−1910